Title

Biochemical and Structural Insights into the Preference of Nairoviral DeISGylases for Interferon-Stimulated Gene Product 15 Originating from Certain Species.

Journal

Journal of Virology, 90(18)

Authors

Deaton, M

Dzimianski, John

Daczkowski, C

et al.

Publication Date

2016-09-15

DOI

10.1128/JVI.00975-16

Peer reviewed

AMERICAN SOCIETY FOR MICROBIOLOGY | Journal of Virology

Biochemical and Structural Insights into the Preference of Nairoviral DeISGylases for Interferon-Stimulated Gene Product 15 Originating from Certain Species

M. K. Deaton,[a] J. V. Dzimianski,[a] C. M. Daczkowski,[a] G. K. Whitney,[a] N. J. Mank,[a] M. M. Parham,[a] E. Bergeron,[b] S. D. Pegan[a]

Department of Pharmaceutical and Biomedical Sciences, University of Georgia, Athens, Georgia, USA[a]; Viral Special Pathogens Branch, Division of High Consequence Pathogens and Pathology, Centers for Disease Control and Prevention, Atlanta, Georgia, USA[b]

ABSTRACT

The regulation of the interferon type I (IFN-I) response has been shown to rely on posttranslational modification by ubiquitin (Ub) and Ub-like interferon-stimulated gene product 15 (ISG15) to stabilize, or activate, a variety of IFN-I signaling and downstream effector proteins. Unlike Ub, which is almost perfectly conserved among eukaryotes, ISG15 is highly divergent, even among mammals. Since zoonotic viruses rely on viral proteins to recognize, or cleave, ISG15 conjugates in order to evade, or suppress, innate immunity, the impact of ISG15 biodiversity on deISGylating proteases of the ovarian tumor family (vOTU) from nairoviruses was evaluated. The enzymatic activities of vOTUs originating from the Crimean-Congo hemorrhagic fever virus, Erve virus, and Nairobi sheep disease virus were tested against ISG15s from humans, mice, shrews, sheep, bats, and camels, which are mammalian species known to be infected by nairoviruses. This along with investigation of binding by isothermal titration calorimetry illustrated significant differences in the abilities of nairovirus deISGylases to accommodate certain species of ISG15. To investigate the molecular underpinnings of species preferences of these vOTUs, a structure was determined to 2.5 Å for a complex of Erve virus vOTU protease and a mouse ISG15 domain. This structure revealed the molecular basis of Erve virus vOTU's preference for ISG15 over Ub and the first structural insight into a nonhuman ISG15. This structure also revealed key interactions, or lack thereof, surrounding three amino acids that may drive a viral deISgylase to prefer an ISG15 from one species over that of another.

IMPORTANCE

Viral ovarian tumor domain proteases (vOTUs) are one of the two principal classes of viral proteases observed to reverse posttranslational modification of host proteins by ubiquitin and interferon-stimulated gene product 15 (ISG15), subsequently facilitating downregulation of IFN-I signaling pathways. Unlike the case with ubiquitin, the amino acid sequences of ISG15s from various species are notably divergent. We illustrate that vOTUs have clear preferences for ISG15s from certain species. In addition, these observations are related to the molecular insights acquired via the first X-ray structure of the vOTU from the Erve nairovirus in complex with the first structurally resolved nonhuman ISG15. This information implicates certain amino acids that drive the preference of vOTUs for ISG15s from certain species.

The majority of emerging viruses in the human population have an origin in an animal reservoir host. Arthropod-borne viruses (arboviruses) are transmitted to vertebrates by blood-feeding arthropods and are a major cause of zoonotic diseases (1). Arboviruses of medical importance include the positive-sense RNA viruses Dengue virus, West Nile virus, Chickungunya virus, and Zika virus and the negative-sense RNA viruses (NSVs) Rift Valley fever virus and Crimean-Congo hemorrhagic fever virus (CCHFV) (2). The recent identification of diverse NSVs suggests that even circulating vertebrate-specific viruses have originated from arthropod virus ancestors, supporting the notion that virus spillovers are the origin of currently circulating vertebrate-restricted viruses (3). Multiple factors contribute to virus spillover events from the reservoir species to other organisms. The type I interferons (IFN-Is) represent one of the first and critical lines of defense against invading viruses and are likely a major obstacle not only for a zoonotic virus's ability to spill over to another organism but also for that organism to become a reservoir itself (1). Not surprisingly, many viral proteins considered to be virulence factors are known to block the innate immune system, enabling viruses to replicate and cause disease.

Initially, a phosphorylation cascade alone was proposed to prompt several features of the IFN-I response, including IFN production and release, the NF-κB inflammation response, and upregulation of several IFN-stimulated gene products with antipathogenic properties (4). However, regulation of the IFN-I response has been shown to go beyond phosphorylation events and also relies on posttranslational modification by ubiquitin (Ub) and Ub-like interferon-simulated gene product 15 (ISG15) (5).

With Ub and ISG15 playing a central role in innate immune

Received 17 May 2016 **Accepted** 29 June 2016

Accepted manuscript posted online 13 July 2016

Citation Deaton MK, Dzimianski JV, Daczkowski CM, Whitney GK, Mank NJ, Parham MM, Bergeron E, Pegan SD. 2016. Biochemical and structural insights into the preference of nairoviral DeISGylases for interferon-stimulated gene product 15 originating from certain species. J Virol 90:8314–8327. doi:10.1128/JVI.00975-16.

Editor: S. Perlman, University of Iowa

Address correspondence to S. D. Pegan, spegan@uga.edu.

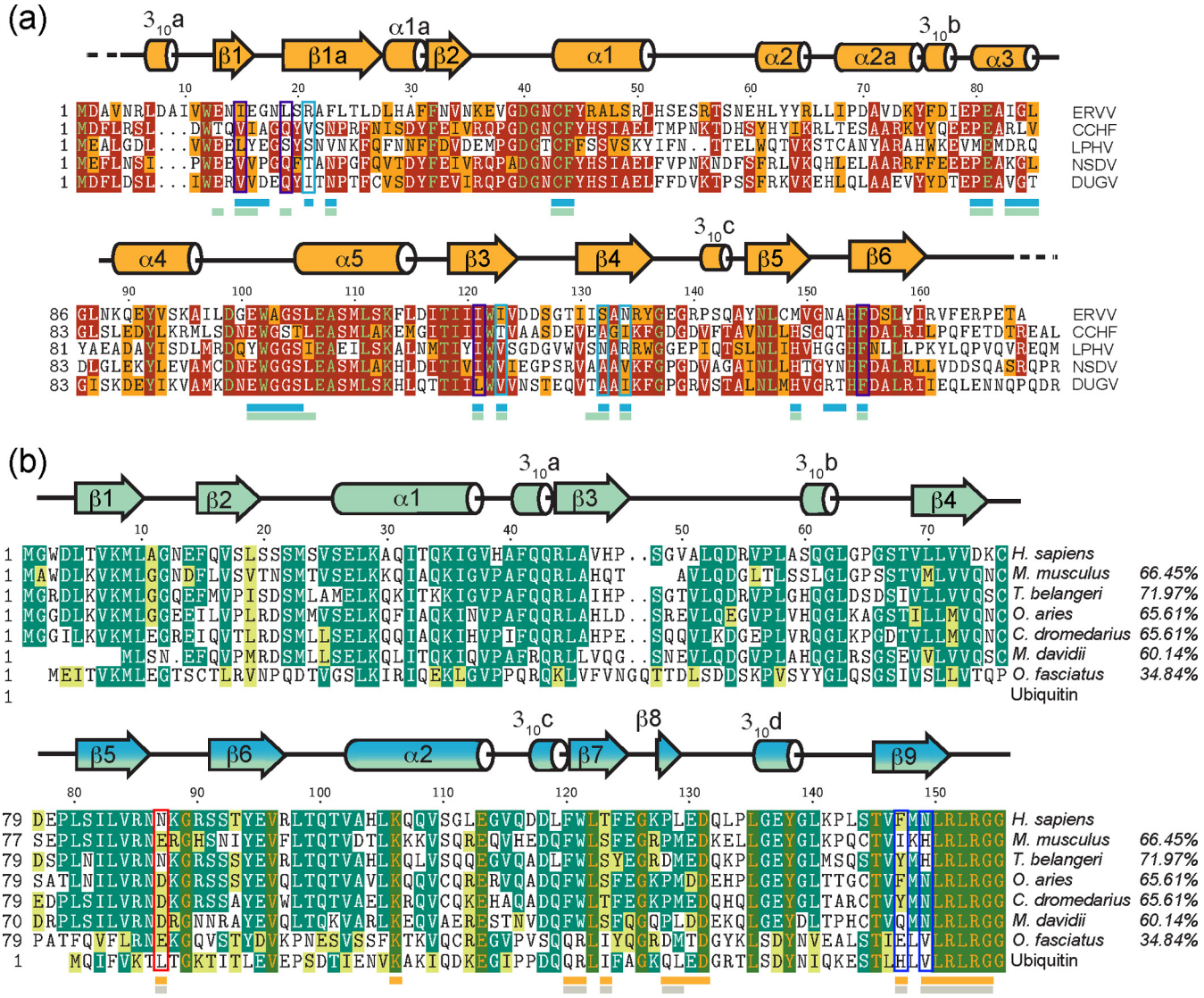

FIG 1 Sequence alignment of vOTUs and ISG15s. (a) The vOTUs from ERVV (GenBank accession no. AFH89032.1), CCHFV (GenBank accession no. AAQ98866.2), and NSDV (GenBank accession no. ACH99799.1), as well as LPHV (GenBank accession no. BAP90971.1) and DUGV (GenBank accession no. AAB18834.1). The secondary structure of ERVV vOTU is shown as α-helices, η-helices (3_{10}-helices), and arrows (β-strands). Residues buried in the ERVV vOTU-CmISG15 structure are indicated by an underlying blue bar, those buried in the CCHFV vOTU-ChISG15 structure by a green bar. Sites corresponding to the RSN motif of ERVV vOTU that was targeted for mutagenesis are boxed in light blue. Conserved hydrophobic valley substrate binding residues in Nairovirus vOTUs are boxed in purple. (b) The ISG15s from *Homo sapiens* (human; accession no. AAH09507.1), *Mus musculus* (mouse; accession no. AAB02697.1), *Tupaia belangeri* (Northern tree shrew; accession no. AFH66859.1), *Ovis aries* (sheep; accession no. AF152103.1), *Camelus dromedarius* (camel; accession no. XP_010997700.1), *Myotis davidii* (vesper bat; accession no. ELK23605.1), and *Oplegnathus fasciatus* (jackknife fish; accession no. BAJ16365.1). Percentages indicate percent identity to human ISG15. The secondary structure of human ISG15 is shown, with human secondary structures colored in green and mouse secondary structures labeled in blue. Residue numbering is based on mouse ISG15. The mouse ISG15 residues buried in the complex with ERVV vOTU are indicated by an underlying orange bar, the human ISG15 residues buried in complex with CCHFV vOTU by a gray bar. The position corresponding to the residue that interacts with the ERVV vOTU RSN pocket implicated in species specificity is boxed in red. Additional residues implicated in species specificity are boxed in royal blue.

regulation, numerous antiviral mechanisms are regulated by the ubiquitination and ISGylation of host and viral proteins. In an effort to undermine a host's ability to mount an effective immune response, viruses are encoding antagonists countering the host antiviral responses mediated by ubiquitination and ISGylation (6–11). Ub represents one of the most conserved eukaryote proteins, whereas ISG15 is absent from invertebrates and highly divergent among mammals, with sequence identities as low as 60% (Fig. 1). This biodiversity of ISG15 has been shown to be a key factor in limiting influenza B virus infection in mice because influenza B virus NS1 cannot bind mouse ISG15, unlike its nonhuman primate and human counterparts (12–14).

The use of influenza A and B virus NS1 proteins to engage ISG15 is not the only viral mechanism that seeks to counter the antiviral activity of ISG15. One of the most direct mechanisms involves viral proteases known as deISGylases, which can reverse the posttranslational modification of host and viral proteins by ISG15. Viral deISGylases have principally been identified in cer-

tain members of the genera *Coronavirus*, *Arterivirus*, and *Nairovirus* (6, 15). For nairoviruses, the deubiquitinase and/or deISGylase activity originates from a viral ovarian domain protease (vOTU) homologue encoded on the large (L) RNA segment of its tripartite genome (6, 16). Unlike positive-sense RNA viruses from the genera *Coronavirus* and *Arterivirus* that require their deubiquitinases and deISGylases to cleave a viral polypeptide for replication, nairoviruses are NSVs requiring no such activity (17). Viruses that are members of the genus *Nairovirus*, of the family *Bunyaviridae*, possess proteases with dedicated, but widely variable, deISGylase and ubiquitinase activities (16).

The majority of nairoviruses are tick-borne pathogens, but they infect vertebrate hosts, resulting in a wide range of species-specific disease outcomes. CCHFV, Erve virus (ERVV), and Nairobi sheep disease virus (NSDV) are nairoviruses that have been implicated in human and other animal diseases. NSDV is a tick-borne nairovirus that causes mild febrile illness in humans but severe disease with a mortality rate of up to 90% in infected animals, such as sheep and goats (18, 19). In humans, CCHFV causes a severe disease that often progresses to fatal hemorrhagic syndrome associated with a mortality rate in humans ranging from 5% to 70% (20, 21). ERVV and other virus from the Thiafora genogroup were isolated from the white-tooth shrew of the genus *Crocidura*. ERVV has been cited as one of the possible causative agents of thunderclap headaches (22). In addition, the brains of mice that have been inoculated with ERVV have shown acute encephalitis and necrosis (23). With no clear tick-borne vector, mice or shrews have been suggested as a reservoir and possible vector for ERVV (24). In addition to causing overt disease in certain species, these nairoviruses have a unique ability to cause viremia in a multitude of other species (25). For example, CCHFV has been experimentally inoculated in sheep, goats, cattle, horses, mice, and hamsters, with no signs of serious disease even with circulating antibodies being detected (25). Serological evidence of ERVV infection in animals, including boar, deer, gulls, sheep, and rodents, has been found (26).

Mirroring the variability of nairoviruses in zoonotic range and disease outcome, vOTUs have also shown variability in terms of substrate preference. In previous studies, nairovirus vOTUs illustrated a capability of operating as deISGylases, deubiquitinases, or both (16). Interestingly, ERVV uniquely employs deISGylases and shows little to no deubiquitinating activity, while CCHFV and NSDV utilize both deISGylases and deubiquitinases. Intriguingly, through indirect means, ERVV vOTU appears to show a greater affinity for mouse ISG15 (mISG15) than its CCHFV counterpart. This has spurred speculation that like NS1 of influenza B virus, the species origin of an ISG15 may also impact the ability of vOTU to cleave corresponding ISG15 conjugates. Regrettably, all of the current studies and structural data available only involve human ISG15 (hISG15). Additionally, there is no mechanism to explain why ERVV encodes a dedicated deISGylase and shows little to no activity as a deubiquitinase or why CCHFV does not prefer to cleave mISG15 (27).

This study aimed to determine the extent and potential sources of ISG15 species specificity within representative vOTUs. As a result, an ISG15 protease activity assay was created in order to determine if vOTUs from different nairoviruses do indeed have a specificity for certain species' ISG15s and if the specificity correlates to the poorly conserved ISG15 sequences. In addition, the first crystal structure of the principally deISGylating vOTU from ERVV not only was revealed but also was captured in complex with the previous structurally uncharacterized C-terminal domain of mouse ISG15. This structure, when compared to the vOTU from CCHFV in complex with C-terminal human, has unlocked key residues that begin to answer the question of species specificity utilized by viral proteases. These insights could serve as the lynchpin in determining how these viruses are able to circumvent certain host innate immune systems that may contribute to virus replication, disease outcome, and persistence in particular host species.

MATERIALS AND METHODS

Construction, expression, and purification of vOTUs. The expression vectors for vOTUs originating from CCHFV and ERVV were constructed according to previously published protocols (16). The NSDV vOTU domain was identified by homology with CCHFV vOTU as the first 169 amino acids (GenBank accession number AED88229.1) of the L protein (6). As with the CCHFV vOTU and other previously described nairovirus vOTU constructs, a 6× histidine tag and a stop codon were appended to the C termini of ERVV vOTU and NSDV vOTU. ERVV vOTU and NSDV vOTU were incorporated into pET11a. All vOTUs were expressed and purified as previously described (16).

Site-directed mutagenesis of ERVV vOTU. ERVV vOTU N134I, S132A, and R21V mutants, along with a triple mutant (N134I/I123T/R21V), were generated using the QuikChange Lightning or QuikChange Lightning Multi site-directed mutagenesis kit according to the manufacturer protocols (Agilent Technologies, Inc.). Mutant plasmids were transformed by heat shock into *Escherichia coli* NEB-5α high-efficiency cells and subsequently propagated and purified. The mutation of the constructs was confirmed by sequencing (Eton Bioscience, Inc.) and the plasmids were transformed into *E. coli* BL21(DE3) by heat shock for protein expression.

ERVV vOTU mutant enzymatic assays. Assays were performed as previously described (16). Briefly, vOTU activity was assessed against ubiquitin-AMC and ISG15-AMC (Boston Biochem, MA) at a final enzyme concentration of 4 nM and a final substrate concentration of 1 μM. Reactions were performed in duplicate in buffer A (100 mM NaCl, 50 mM HEPES [pH 7.5]), 0.01 mg/ml of bovine serum albumin, and 5 mM dithiothreitol (DTT) using a 96-well Corning Costar half-volume plate with a 50-μl total reaction volume. Reaction rates were assessed by measuring the fluorescence generated by the cleavage of 7-amino-4-methylcoumarin from the substrate using a CLARIOstar plate reader (BMG Labtech, Inc.). Data analysis was performed using MARS (BMG Labtech).

Construction, expression, and purification of proISG15s and mature ISG15s. ISG15s from human (*Homo sapiens*; accession number AAH09507.1), mouse (*Mus musculus*; accession number AAB02697.1), northern tree shrew (*Tupaia belangeri*; accession number AFH66859.1), sheep (*Ovis aries*; accession number AF152103.1), dromedary camel (*Camelus dromedarius*; accession number XP_010997700.1), vesper bat (*Myotis davidii*; accession number ELK23605.1), and jackknife fish (*Oplegnathus fasciatus*; accession number BAJ16365.1) (all accession numbers are for GenBank) were identified by sequence homology. A mutation (C75S) was made in the mouse sequence to prevent aggregation. This change was also made in all sequences sent for gene synthesis. The C-terminal domains of the mature ISG15s were appended with GTEPGG RSGHHHHHH, which corresponds to the C terminus of the immature human ISG15 (proISG15) sequence with a 6× histidine tag. Gene synthesis was carried about by Genscript (Piscataway, NJ). Mature ISG15s were made by the introduction of a stop codon after the C-terminal RLRGG motif of the proISG15s.

All ISG15 constructs were grown at 37°C in LB broth containing 100 μg/ml of ampicillin to an optical density at 600 nm (OD_{600}) of 0.6 to 0.8 and induced by the addition of 0.8 mM isopropyl-β-D-thiogalactopyranoside (IPTG). The cultures were then grown for 4 h at 37°C. The cells were then pelleted by centrifugation at 6,000 × *g* for 10 min and frozen at

−80°C until use. ProISG15s were lysed in buffer B {500 mM NaCl, 50 mM Tris [pH 7.5], 1 mM Tris (2-carbozyethyl) phosphine hydrochloride [TCEP-HCl]} and 5 mg of lysozyme for 45 min at 4°C and sonicated on ice at 50% power with 5-s pulse increments for 6 min. Insoluble protein was removed by centrifugation at 48,000 × *g* for 45 min. The clarified supernatant was filtered with a 0.80-μm filter and flowed over high-density nickel agarose beads (GoldBio) equilibrated with buffer B. The protein column was washed with buffer B supplemented with 30 mM imidazole and then eluted with buffer B supplemented with 300 mM imidazole. The resulting protein elution was dialyzed overnight at 4°C in 200 mM NaCl and 50 mM HEPES (pH 8.0).

Mature ISG15s were lysed in buffer C (500 mM NaCl, 50 mM Tris [pH 8.0], 10 mM imidazole) and 5 mg of lysozyme for 45 min at 4°C. The solution was sonicated on ice at 50% power with 5-s pulse increments for 6 min. The cell debris was pelleted by centrifugation at 48,000 × *g* for 30 min, and the supernatant was filtered through a 0.80-μm filter. The supernatant was then flowed over high-density nickel agarose beads (GoldBio) equilibrated with buffer C and then washed with buffer C supplemented with 30 mM imidazole, followed by elution with buffer C supplemented with 300 mM imidazole. The mature ISG15s were then dialyzed into 50 mM HEPES [pH 8.0] and 150 mM NaCl, thrombin cleaved, and purified by size exclusion chromatography using a Superdex S200 column (GE Healthcare, Piscataway, NJ). Fractions containing ISG15 were concentrated and dialyzed against a buffer containing 50 mM HEPES, 150 mM sodium chloride, and 5 mM β-mercaptoethanol.

ISG15 protease activity assay. Briefly, 10 μM purified northern tree shrew proISG15 (pro-nsISG15), sheep proISG15 (pro-shISG15), fish proISG15 (pro-fISG15), mouse proISG15 (pro-mISG15), camel proISG15 (pro-cISG15), bat proISG15 (pro-bISG15), or human proISG15 (pro-hISG15) was incubated with a 20 nM concentration of either CCHFV vOTU, ERVV vOTU, or NSDV vOTU at 37°C in 200 mM NaCl, 5 mM HEPES (pH 7.5), and 2 mM DTT. The reactions were stopped at various time points (0, 1, 2, 5, 10, 30, and 60 min) by mixing 9 μl of each reaction mixture with equal parts 2× SDS-Tricine sample buffer, followed by boiling at 98°C for 5 min. The results were visualized on 10 to 20% Mini-PROTEAN Tris-Tricine precast gels (Bio-Rad, Hercules, CA).

ITC of ISG15 with vOTUs originating from ERVV and CCHFV. Isothermal titration calorimetry (ITC) was performed using a Microcal PEAQ-ITC (Malvern, Worcestershire, United Kingdom). There were 18 injections of 2 μl each at 25°C with a reference power of 10 μcal/s. The ISG15s and vOTUs were dialyzed at 4°C in 50 mM HEPES (pH 7.5), 150 mM NaCl, and 5 mM β-mercaptoethanol. All experiments were run in duplicate. The proteases were in the cell at concentrations of 100 to 150 μM with a 1 to 1.5 mM concentration of the selected ISG15 in the syringe. The data were processed using Microcal PEAQ-ITC analysis software.

ERVV vOTU-CmISG15 complex formation. The C-terminal domain of mISG15 (CmISG15) in expression vector pTYB2 was lysed with buffer D (25 mM HEPES [pH 6.8], 50 mM sodium acetate, and 75 mM NaCl augmented with 0.16% Triton X-100). The solution was sonicated on ice at 50% power with a 50% duty cycle for 10 min. Cellular debris was removed by centrifugation methods at 17,000 × *g* for 45 min. The clarified supernatant was filtered with a 0.80-μm filter and then poured over a chitin column preequilibrated with buffer D. The column was then washed with three column volumes of buffer D and resuspended in two column volumes of buffer D supplemented with 250 mM sodium 2-mercaptoethanesulfonate (MESNA). The resuspension was rocked gently at 4°C overnight, and the chitin beads were collected by gravity flow. The resulting CmISG15 thioester was concentrated to reduce the total volume to 20 ml. A total of 480 μl of 5 M NaOH and 1.84 g of propargylamine were added to the CmISG15 thioester and left to incubate overnight at 4°C, resulting in the derivatized product (CmISG15-PA).

Synthesis of the CmISG15 complex was adapted from previously described methods (28–30). Briefly, to obtain the ERVV vOTU-CmISG15 complex, purified protease was added directly to the mixture in equimolar ratios, incubated for 2 to 4 h at room temperature, and left at 4°C overnight. To further purify the complex, anion-exchange chromatography was used, eluting from a MonoQ 10/100 column using a linear gradient from 0 to 1 M NaCl with 50 mM Tris (pH 7.3), followed by size exclusion chromatography on a Superdex 75 column (GE Healthcare, Pittsburgh, PA) preequilibrated with 100 mM NaCl, 5 mM HEPES (pH 7.5), and 2 mM DTT.

TABLE 1 Data collection and refinement statistics

Parameter	Value for ERVV vOTU-CmISG15 (5JZE)
Data collection statistics	
Space group	$P4_3$
Cell dimensions	
a, *b*, *c* (Å)	66.0, 66.0, 122.0
α, β, γ (°)	90.0, 90.0, 90.0
Resolution (Å)	50.00–2.47 (2.51–2.47)[a]
R_{sym} or R_{merge}	0.12 (0.48)
$I/\sigma I$	11.5 (2.56)
Completeness (%)	100.0 (100.0)
Redundancy	4.2 (3.7)
Refinement statistics	
Resolution (Å)	66.0–2.47
No. of reflections	17,722
R_{work}/R_{free}	0.174/0.226
No. of atoms	
Protein	3,829
Ligand/ion	60
Water	253
B factors	
Protein	24.4
Ligand/ion	53.1
Water	23.1
RMSD[b]	
Bond lengths (Å)	0.014
Bond angles (°)	1.71

[a] Values in parentheses are for highest-resolution shell.
[b] RMSD, root mean square deviation.

Crystallization of ERVV vOTU-CmISG15. The ERVV vOTU-CmISG15 complex was screened at 12.5 mg/ml against a series of Qiagen NeXtal suites by hanging drop using a TTP Labtech Mosquito (TTP Labtech, Herfordshire, United Kingdom). The initial screens yielded needle-like crystals from a condition containing 6% polyethylene glycol 6000 (PEG 6000) and 0.1 M citric acid [pH 4.6]. This condition was optimized using a Hampton Research Additive HT Screen. The final optimized crystals were grown in hanging drops with 2 μl of protein solution mixed 1:1 with mother liquor containing 6% PEG 6000 and 0.1 M citric acid supplemented with 0.2 μl of 3.0 M NTSB-195. The crystals were flash frozen in a cryoprotective solution containing 30% PEG 6000 and 0.1 M citric acid [pH 4.6] and mounted under a dry N_2 stream at 100 K. A data set was collected at the Advanced Photon Source (Argonne National Labs, Argonne, IL) on SER-CAT beamline BM-22 using a MAR300hs detector. Data were collected using a wavelength of 1 Å.

Data processing and structure solutions. The data set was indexed, integrated, and scaled using HKL-2000 (31). The structure was solved by molecular replacement using Phaser (32). The ERVV vOTU-CmISG15 complex was solved using a homology model based on a vOTU-ubiquitin complex (PDB entry 4HXD). Successive rounds of manual model building and refinement were done using Coot (33) and Refmac5 from the CCP4 suite. The final model was validated using CCP4 suite (34) programs Procheck and Sfcheck. The final structure was deposited with the Protein Data Bank (5JZE) with statistics in Table 1.

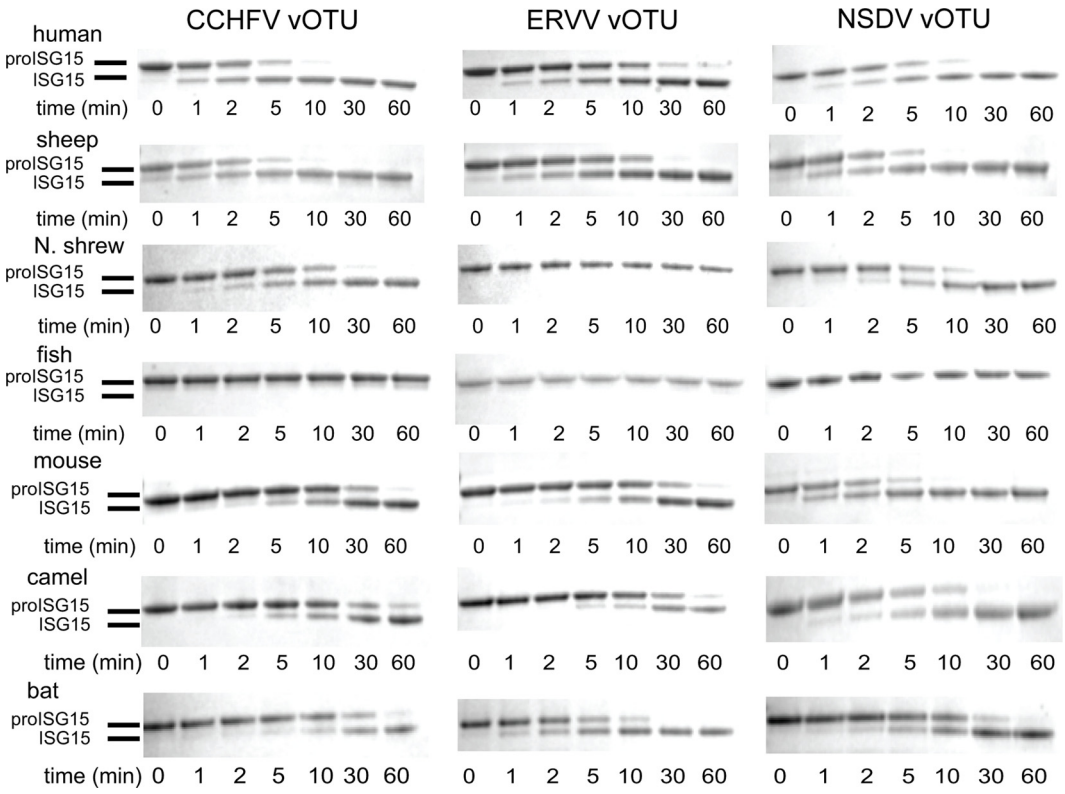

FIG 2 ISG15 protease activity assay of vOTU proISG15 cleavage specificity. CCHFV vOTU, ERVV vOTU, and NSDV vOTU were evaluated for cleavage of human, sheep, northern tree shrew, fish, mouse, camel, and bat proISG15. A 10 μM concentration of each proISG15 was incubated with a 20 nM concentration of each vOTU at 37°C for at least 1 h, with samples taken at the time points indicated.

RESULTS

Cleavage of proISG15s by vOTUs. With ISG15 homologues sharing low sequence identity among mammals that are frequently exposed to zoonotic nairoviruses encoding deISGylases, the effect of this species diversity on viral deISGylase function was examined. With no suitable assays to rapidly assess the impact interspecies sequence diversity of ISG15s has on viral deISGylase activity, an assay was developed leveraging the ability of these proteases to cleave immature forms of ISG15 (27). Naturally, the immature form of ISG15 may not be the most naturally pertinent substrate for viral deISGylases; however, this setup provides a manner in which to rapidly screen for differences between ISG15s from numerous species without the need for extensive chemical synthesis or knowledge pertaining to the identity of ISG15-specific E1 ligases within the species being investigated (35).

For the ISG15 protease assay, homologues of hISG15 from species that have been proposed as hosts for deISGylase-containing viruses, or closely related to those species, were chosen. Specifically, species included human (pro-hISG15), sheep (pro-shISG15), northern tree shrew (pro-nsISG15), dromedary camel (pro-cISG15), and mouse (pro-mISG15) in relation to NSDV, ERVV, and CCHFV. Vesper bat (pro-bISG15) was also included, as multiple nairoviruses and even CCHFV appears to infect certain bat species (36–38). In order to include an ISG15 with lower sequence identity than 60%, a distant homologue of human ISG15 from jackknife fish was also included (pro-fISG15). To focus the assay on detecting difference originating from the mature ISG15 component of the substrate, the C-terminal sequence from immature hISG15 comprised the immature portion of all the pro-ISG15 substrates. Samples were collected at intermittent time points over the course of an hour, and cleavage was determined by SDS-PAGE.

Utilizing this assay, vOTUs possessing, or suspected of possessing, robust deISGylase activity from CCHFV, ERVV, and NSDV were examined for the ability to cleave pro-ISG15s (Fig. 2). Surprisingly, a wide range of diversity of cleavage patterns was observed. CCHFV vOTU processes human and sheep pro-ISG15s rapidly, with all of these pro-ISG15s cleaved within a 10-min time frame. CCHFV vOTU also appears to have the ability to process pro-ISG15 from the northern tree shrew. Similar to CCHFV vOTU, ERVV vOTU also robustly cleaves the pro-forms of hISG15 and shISG15, albeit slightly slower than CCHFV vOTU. As suggested by a previous report, CCHFV vOTU cleaves pro-mISG15 markedly less than for its human counterpart, whereas ERVV vOTU appears process pro-mISG15 faster than CCHFV vOTU but still slower than pro-hISG15 (16). Intriguingly, the substrate preference of vOTUs from ERVV and CCHFV differ for pro-ISG15 forms from northern tree shrew and vesper bat. There is an absence of activity of ERVV vOTU for ISG15 from the northern tree shrew. However, it does possess the ability to cleave the pro-bISG15. CCHFV vOTU has the reverse activity, preferring the pro-nsISG15 to the pro-bISG15. Unlike the vOTUs from CCHFV and ERVV, NSDV vOTU has a significantly broader range of activity. As expected, NSDV vOTU has the most activity toward pro-shISG15 but also has robust activity toward the pro-forms of hISG15 and mISG15. In addition, it also has moderate activity

TABLE 2 ITC results for ISG15 binding to CCHFV vOTU and ERVV vOTU[a]

Protein	N[b] (sites)	K_D (μM)	ΔH^c (kJ/mol)	ΔG^d (kJ/mol)	$-T\Delta S^e$ (kJ/mol)
ERVV vOTU					
Human	0.944 ± 0.004	0.36 ± 0.05	−32.20 ± 0.35	−36.8	−4.67
Sheep	0.970 ± 0.003	1.05 ± 0.05	−30.80 ± 0.149	−34.2	−3.35
Mouse	0.956 ± 0.004	7.48 ± 0.26	−28.30 ± 0.20	−29.3	−1.00
CCHFV vOTU					
Human	0.935 ± 0.032	3.51 ± 1.30	6.00 ± 0.41	−31.2	−37.2
Sheep	0.897 ± 0.007	1.80 ± 0.24	−14.10 ± 0.23	−32.8	−18.7
Mouse	0.993 ± 0.074	72.00 ± 27.10	8.30 ± 1.46	−23.7	−32.0

[a] The ITC results for CCHFV vOTU and ERVV vOTU are shown. The ISG15s were placed in the syringe at a 10-fold-higher concentration than the protease in the cell.
[b] Binding stoichiometry.
[c] Binding enthalpy.
[d] Gibb's free energy.
[e] Entropy factor.

toward the pro-forms of cISG15, nsISG15, and bISG15. NSDV vOTU only fails to cleave the pro-form of fISG15, which is not cleaved by any of the vOTUs assessed.

Thermodynamics of ISG15 binding to nairovirus vOTUs. Based on the divergence of activity observed by several of the viral deISGylases, isothermal titration calorimetry (ITC) was employed to gain a better sense of scale related to the differences observed in the protease assay. In addition, this also was used to provide a thermodynamic perspective of the ability of ISG15s to bind to representative vOTU members. Specifically, CCHFV vOTU or ERVV vOTU were added to the cell and were titrated with mature forms of mISG15, hISG15, or shISG15 in the injector (Table 2; Fig. 3). The binding stoichiometry was 1:1 between the proteases and the ISG15s. Both endothermic and exothermic interactions were observed, suggesting multiple modes of binding between the ISG15s and the proteases. While CCHFV vOTU has been shown to bind Ub in an entropically driven manner (39), its interactions with ISG15s ranged from exothermic for shISG15 and endothermic for hISG15 and mISG15. The highest affinity was seen for hISG15 and shISG15, with K_Ds (equilibrium dissociation constants) of 3.51 ± 1.30 and 1.80 ± 0.24 μM. The binding of mISG15 was more than 20-fold weaker, with a K_D of 72.00 ± 27.10 μM. These results mirror the differences observed in the ISG15 protease activity assay, illustrating the magnitude of affinity difference between human and sheep ISG15s for CCHFV vOTU. Unexpectedly and unlike CCHFV vOTU, ERVV vOTU was exothermic for all of the ISG15s and had the lowest overall K_Ds, suggesting that hydrophobic interactions play a diminished role in ERVV vOTU binding of ISG15s. ERVV vOTU also possessed the lowest K_D seen for the ISG15s tested, with its K_D for hISG15 at 0.36 ± 0.05 μM. Its affinity for shISG15 was not much higher, with a K_D of 1.05 ± 0.05 μM. As expected from the ISG15 protease activity assay, affinity for mISG15 was significantly lower, with a K_D of 7.48 ± 0.26. However, this was 10-fold tighter than CCHFV vOTU's affinity for mISG15. Overall, the affinities of ISG15 by ITC not only parallel the results of the ISG15 protease assay but also provide quantitative insight into the substantial differences in those affinities.

Structure of ERVV vOTU. With the notable differences observed in the enzymatic activity of vOTUs for ISG15s originating from different species and the thermodynamic manner in which they bind them, molecular insights into this phenomenon were sought. To this end, the C-terminal domain of mISG15 (CmISG15) was covalently linked to ERVV vOTU via a vinyl thioether (ERVV vOTU-CmISG15). The covalent complex crystallized in space group $P4_3$, and the structure was determined at a resolution of 2.47 Å. Within the asymmetric unit, two copies of the ERVV vOTU-CmISG15 complex were observed.

Globally, the vOTU from the ERVV adopts a familiar vOTU fold of a central seven-stranded β-sheet flanked by five α-helices. These elements form a cleft in which the CmISG15 substrate is bound (Fig. 4a and b). Comparing ERVV vOTU with its CCHFV counterpart, one area of particular interest is immediately apparent, providing insight not only into the ERVV vOTU's substrate preferences, but also into vOTUs at large. Specifically, the substrate interface of ERVV vOTU is considerably more charged than that of CCHFV vOTU (Fig. 4c and d). Several residues were identified by homology to be responsible for this change: Arg21/Val18, Ser132/Ala129, and Asn134/Ile131 from ERVV/CCHFV, respectively (Fig. 4d). The presence of this RSN motif within ERVV vOTU lines up with the thermodynamic observations that hydrophobic interactions play a more minor role in ERVV vOTU substrate binding than that of CCHFV vOTU (Table 2). In short, this pocket in CCHFV vOTU accommodates Leu8 of Ub, which corresponds to Glu87 of CmISG15 and in general is found to be either a polar or acidic residue within ISG15s (Fig. 1 and 4e). As a result, this ERVV vOTU surface appears to be at odds in accommodating Leu8 of Ub and likely is one of the major contributing factors in the lack of deubiquitinase activity found in ERVV vOTU.

To evaluate the role of this pocket in determining selectivity for ISG15 versus ubiquitin, mutations were introduced into ERVV vOTU and the effect was measured enzymatically. Single mutants consisting of S132A, N134I, and R21V were constructed along with a triple mutant containing R21V/I123T/N134I. Activity for each mutant toward a 7-amino-4-methylcoumarin conjugate with human ISG15 (hISG15-AMC) and ubiquitin (Ub-AMC) was measured and compared against wild-type ERVV vOTU (Fig. 4f). In contrast to S132A, which had a minimal effect, N134I and R21V each increased activity toward Ub-AMC 15- and 20-fold, respectively. For R21V, there was a corresponding reduction in activity toward hISG15-AMC by an order of magnitude. The triple mutant showed activity toward Ub-AMC similar to that of the R21V mutant, with a partial recovery of activity toward hISG15-AMC. This suggests that the presence of the RSN motif is a key driver in determining a vOTU's preference for Ub.

Structure of CmISG15. In addition to identifying key differ-

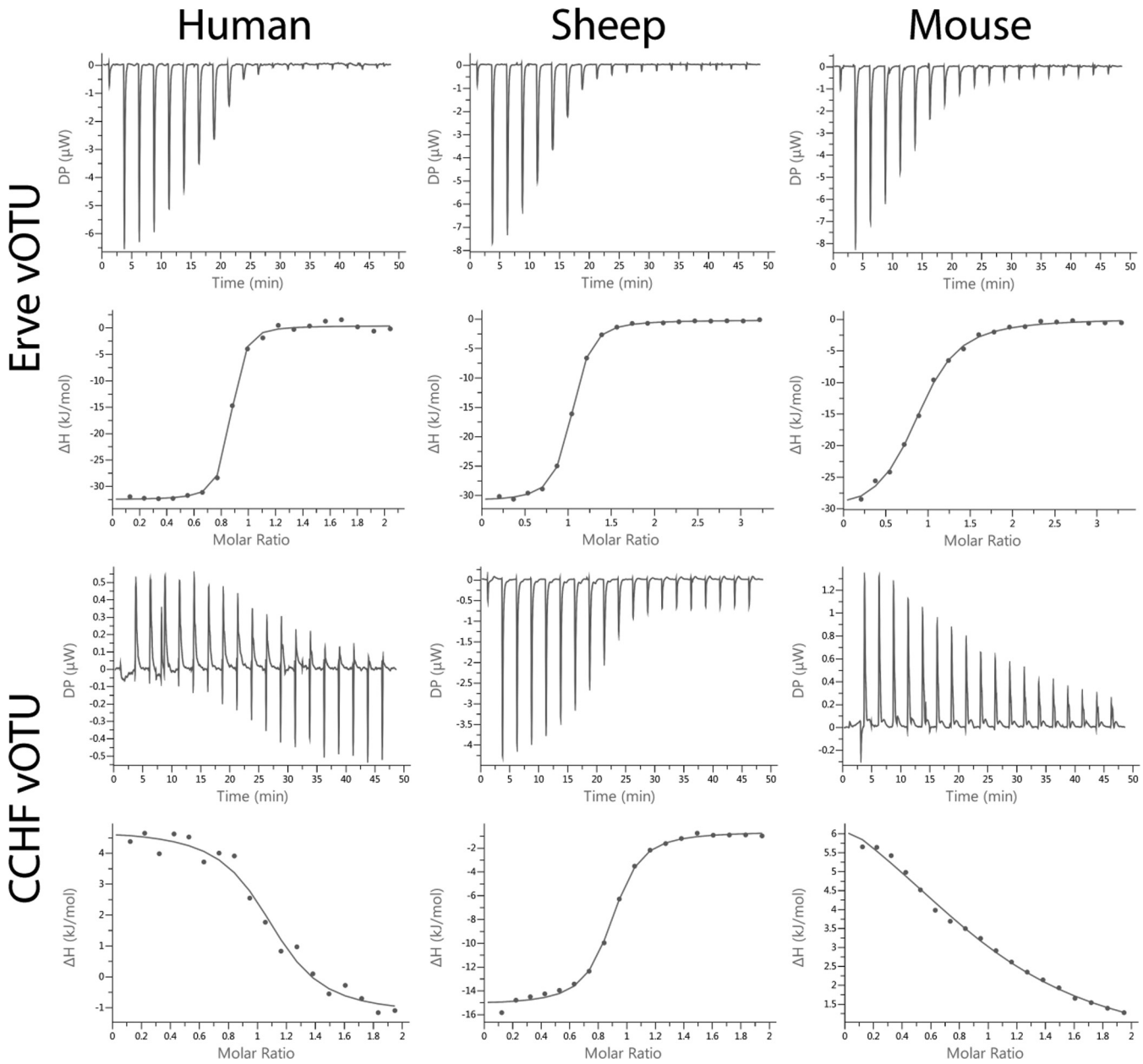

FIG 3 Typical ITC binding isotherms with the raw heat (top panel) and the integrated heats of injection (bottom panel) shown for each interaction.

ences between ERVV vOTU and other nairovirus vOTUs with dual activities or principally deubiquitinase activity, the ERVV vOTU-CmISG15 structure provides the first structural insight into a nonhuman ISG15. Broadly, the CmISG15 domain shares the same secondary structure composition of Ub and the C-terminal domain of hISG15 consisting of five β-sheets and one α-helix. Similar to Ub and the C-terminal domain of hISG15, 3_{10} helices are present between the α-helix and sheet 7 as well as between sheets 8 and 9 (Fig. 1 and 5a). An overlay of CmISG15 with the C-terminal domain of hISG15 illustrates that the tertiary fold is also conserved (Fig. 5b). However, this is where the similarity largely ends.

Although ISG15s originating from both humans and mice share a hydrophobic patch centered around a well-conserved tryptophan at positions 123 and 121, respectively, mISG15 has an additional hydrophobic path located around Phe97. Unlike mISG15, its human counterpart has a strong positively charged surface centered around Arg99. Intriguingly, this region within hISG15 has been shown to form domain-domain interactions with the N-terminal lobe, suggesting that mISG15's domain-domain interactions potentially differ from those observed in hISG15.

When the surface of CmISG15 is viewed from an electrostatic perspective, differences beyond the presence of the hISG15's Arg99-centric positive patch become apparent (40). Overall, the ChISG15 surface has very defined positive, negative, and neutral patches. However, the charges found on the CmISG15 surface are more uniformly distributed. For example, in hISG15 a positive

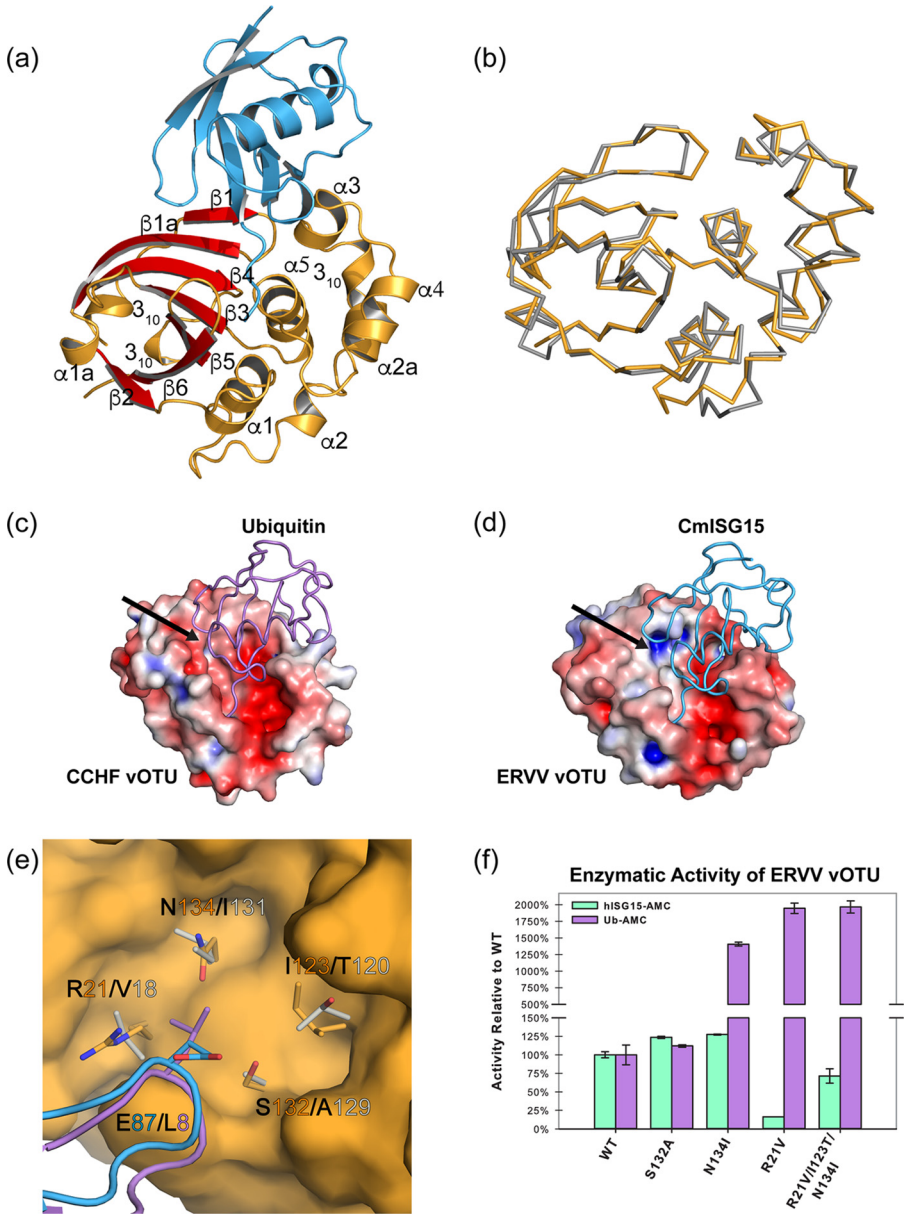

FIG 4 Structure of ERVV vOTU complexed with CmISG15. (a) Cartoon representation of ERVV vOTU (gold) bound to CmISG15 (blue). Helical regions are rendered in gold and β-sheets in red, with each numbered sequentially. (b) Comparison of ERVV vOTU (orange) and CCHFV (gray) shown as ribbons. (c) Electrostatic surface of CCHFV vOTU bound to Ub (lavender) with Ub depicted as a ribbon. Calculations were performed using the PDB2PQR server and surface generated using the adaptive Poisson-Boltzmann solver (APBS). The arrow indicates the location of the hydrophobic binding pocket. (d) Electrostatic surface of ERVV vOTU bound to CmISG15 (blue), with CmISG15 depicted as a ribbon, generated as for panel b. The arrow indicates the location of the hydrophobic binding pocket. (e) The hydrophobic binding pocket of ERVV vOTU (orange) identified from the electrostatic surface. CmISG15 (light blue) and Ub (lavender) are included for comparison. (f) Activity of ERVV vOTU mutants relative to that of the wild type against hISG15-AMC (green) and Ub-AMC (lavender).

ridge is present starting close to its C terminus with Arg155 and continuing along Arg153, Asn151, Asn89, and Arg87, with contributions from Phe149. In contrast, this surface is broken up in mISG15 by Ile147 and His149 in lieu of hISG15's Asn151 and Phe149 (Fig. 5c and d).

Intriguingly, many of the electrostatic differences between the surfaces of the ISG15s of mice and humans appear not to be due solely to the substitution of one surface facing side chain in lieu of another. For instance, previous structural studies on hISG15 highlighted an anionic ridge running throughout hISG15 (Fig. 5d) (41). In ChISG15, this ridge is made up of Glu139, Glu132, Asp133, Asp119, and Asp120 (Fig. 5d, right side). While CmISG15 possesses analogous residues, its surface charge distribution forms a truncated form of this acidic ridge (Fig. 5c). This truncation occurs by the presence of mISG15 His116 in place of Gln118 in hISG15. This substitution creates a substantially different hydrogen bond network in the region than that observed in hISG15. Specifically, in the reported CCHFV vOTU-hISG15 complexes, the oxygen on the side chain of Gln118 is well within hydrogen bonding distance of Glu120, suggesting that the alternative rota-

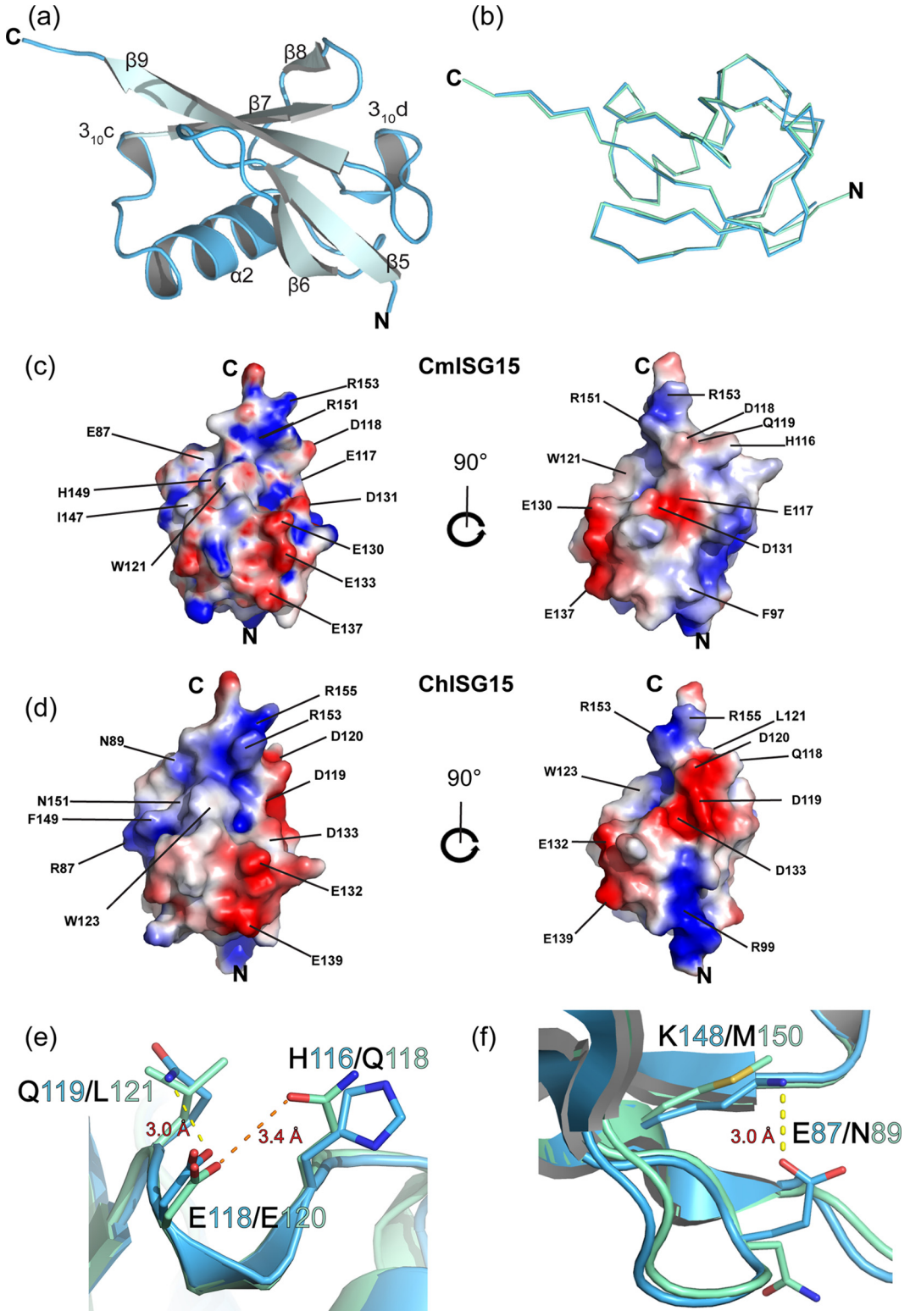

FIG 5 Comparison of mISG15 and hISG15. (a) Secondary structure of CmISG15 (blue) with β-sheets colored in silver. (b) Overlay of CmISG15 (blue) with ChISG15 (green) from the CCHFV vOTU-bound complex (PDB entry 3PHX) shown as ribbons. (c) Electrostatic surface of CmISG15. Calculations were performed using the PDB2PQR server and the surface generated using the adaptive Poisson-Boltzmann solver (APBS). (d) Electrostatic surface of ChISG15 from CCHFV vOTU-ChISG15 (PDB entry 3PHX), generated as for panel c. (e) Residue differences between CmISG15 (blue) and ChISG15 from 3PHX (green) that impact the surface potential. Side chains are shown as sticks, with hydrogen bonding as yellow dashes. (f) Differences in intramolecular interactions between CmISG15 (blue) and hISG15 (green) from CCHFV vOTU-hISG15 (PDB entry 3PSE) that impact the binding surface.

mer configuration is more likely in those structures (42, 43). However, in mISG15 the equivalent glutamate, Glu118, prefers to form a hydrogen bond with the amide of Gln119 (Fig. 5e). Another similar indirect change occurs at position 148 in mISG15. This lysine occupied position is typically a methionine or other hydrophobic residue in other ISG15s. Although not immediately present on the surface, this internal difference between mISG15 and hISG15 allows for a hydrogen bond to form between mISG15 residues Lys148 and Glu87. This has the impact of reorienting the position of Glu87 compared to its human counterpart Asn89 away from the surface (Fig. 5f).

ERVV vOTU-CmISG15 interface. The ERVV vOTU-CmISG15 interface spans 907.9 Å^2 and is comprised of a mix of hydrophobic, hydrogen bond, and charged mediated interactions (Fig. 5). Surprisingly, despite the predominantly electrophilic surface of the Erve vOTU substrate binding site, there are very few salt bridges. The most notable salt bridge is mISG15 residue Arg153 interacting with ERVV vOTU residue Glu101. Beyond this interaction, the majority of the electrostatic interactions are involved in water-mediated hydrogen bonding networks. CmISG15 residues form direct and water-mediated hydrogen bonding networks involving the main chain or side chains of mISG15 residues Gly154, Arg153, Leu152, Arg151, Leu150, and Gln119 with ERVV vOTU residues Glu101, Glu107, Asn152, Asn134, Ser105, and Glu81 (Fig. 5).

These types of electrophilic interactions surround three areas of hydrophobic interactions. One of these is formed by mISG15 Pro128 inserting into a hydrophobic cavity of ERVV vOTU formed by Ile83 and Pro80. The second involves mISG15's Ile147 and elements of His149 packing with the Ile15 of ERVV vOTU. The third appears to serve as the basis for the sole major tertiary fold difference between CCHFV vOTU and ERVV vOTU (Fig. 4b). Specifically, this tertiary structural difference is observed between the vOTUs of CCHFV and ERVV originating in the α3-helix. From a primary structure perspective this suitably named selectivity helix is weakly conserved among nairovirus vOTUs (Fig. 1a) (16). Within the structure of the Dugbe nairovirus vOTU, this helix was observed to be flexible and a key factor in that vOTU's inability to cleave ISG15 conjugates. Intriguingly, alternate orientations of α3 appear to be driven by an effort to provide a hydrophobic pocket for accommodation of the ISG15s' well-conserved Trp121 (Fig. 6c). In the ERVV vOTU-CmISG15 complex, the alkyl side chain portion of the protease's Glu81 and backbone between this residue and Pro80 creates the floor of this pocket. The Glu81 also facilitates a water-mediated hydrogen bond network involving the indole nitrogen of CmISG15's Trp121. ERVV vOTU's Pro80 closes off one side of the pocket. This is a composition similar to that found in CCHFV vOTU. However, the manner in which each of these vOTUs forms the other wall of the pocket is interesting. Both utilize a leucine; however, the origin of the leucine within the helix differs greatly. This suggests that the tertiary structural divergence between the α3 of ERVV and CCHFV vOTUs is likely driven in a manner to ensure that the well-conserved Trp121 of ISG15s can be accommodated by this Pro-Glu-Leu-formed pocket.

DISCUSSION

Molecular insights into substrate specificity in ERVV vOTU and other similar nairovirus vOTUs. Prior to the identification of ERVV vOTU as a deISGylase, viral proteases had either been identified as deubiquitinases or possessed both deubiquitinase and deISGylase activities (16). Intriguingly, the structure of ERVV vOTU reveals the basis for this protease's unique substrate specificity for ISG15s. Similar to vOTUs from CCHFV and Dugbe virus (DUGV), ERVV vOTU contains a number of hydrophobic residues, Ile15, Leu19, Ile121, and Phe155, that can create a hydrophobic valley at the bottom of its ubiquitin binding motif (Fig. 1). These residues are relatively highly conserved among all known nairovirus vOTUs. Although ERVV vOTU includes this motif, suggesting that it too would be able to accommodate Ub's conical Ile44 centric hydrophobic patch, the hydrophobic valley's presence appears not to be sufficient to infer robust deubiquitinase activity (Fig. 1) (16). In light of the mutational evidence of ERVV vOTU's RSN motif, this feature is the principal obstacle to ERVV vOTU possessing deubiquitinase activity.

Intriguingly, among the nairoviruses, this motif had not been previous observed when ERVV vOTU was identified, suggesting that ERVV vOTU may have been a unique member of the vOTU family. However, recently a nairovirus, Leopards Hill virus (LPHV), was isolated from giant leaf-nosed bats (*Hipposideros gigas*) in 2010-2011 (44). Surprisingly, within the LPHV vOTU a comparable electrophilic SNR motif is present, signifying the likelihood that similar motifs may be present in other unknown nairoviruses (Fig. 1). Naturally, whether this vOTU or others possessing similar motifs have robust deISGylase activity would be an open question. However, in light of the impact of the RSN motif in ERVV vOTU, analogous motifs present in other vOTUs would suggest that they are unlikely have robust deubiquitinase activity.

Divergence between the vOTUs of ERVV and CCHFV in accommodating mISG15. Beyond the electrophilic nature of the pocket that encompasses the RSN motif, there are numerous other electrophilic interactions within the interface of the ERVV vOTU-CmISG15 complex. At first glance, this is not very surprising given the mixed charged surface previously observed in hISG15 as well as the enthalpic nature of hISG15 and mISG15 observed via ITC. However, unlike the previously observed CCHFV vOTU-hISG15 structures where these interactions are almost entirely direct residue-to-residue interactions, the ERVV vOTU-CmISG15 structure is based almost solely on water-mediated hydrogen bond interactions (Fig. 6). Taking into consideration that ERVV vOTU still possesses the ability to engage the well-conserved ISG15 Trp123 through the flexibility of its α3 selectivity helix, the presence of other conserved hydrophobic interactions, and ERVV vOTU's lower K_D for hISG15, the binding strength of this network appears significantly robust.

In addition to illustrating a higher affinity for hISG15, this water-mediated hydrogen bond network appears to offer an affinity for binding mISG15 that is an order of magnitude greater. Comparison of the ERVV vOTU-CmISG15 with those of CCHFV vOTU-hISG15 appears to offer some insights into CCHFV vOTU's weaker affinity for mISG15 (Fig. 7a). Centric to the interfaces of the CCHFV vOTU-hISG15 and ERVV vOTU-ISG15 complexes are three ISG15 positions. In hISG15 they encompass Asn89, Phe149, and Asn151. Strikingly, their counterparts in mISG15 are Glu87, Ile147, and His149, respectively. The impacts across the interface appear to be multifold. CCHFV vOTU uses Glu128 to form a hydrogen bond with hISG15 Asn89. However, driven by the substitution of a lysine for methionine residue at mISG15 position 148 coupled to the longer negatively charged side chain of glutamate at mISG15 position 87, the ability of a comparable CCHFV vOTU-mISG15 hydrogen bond to form is

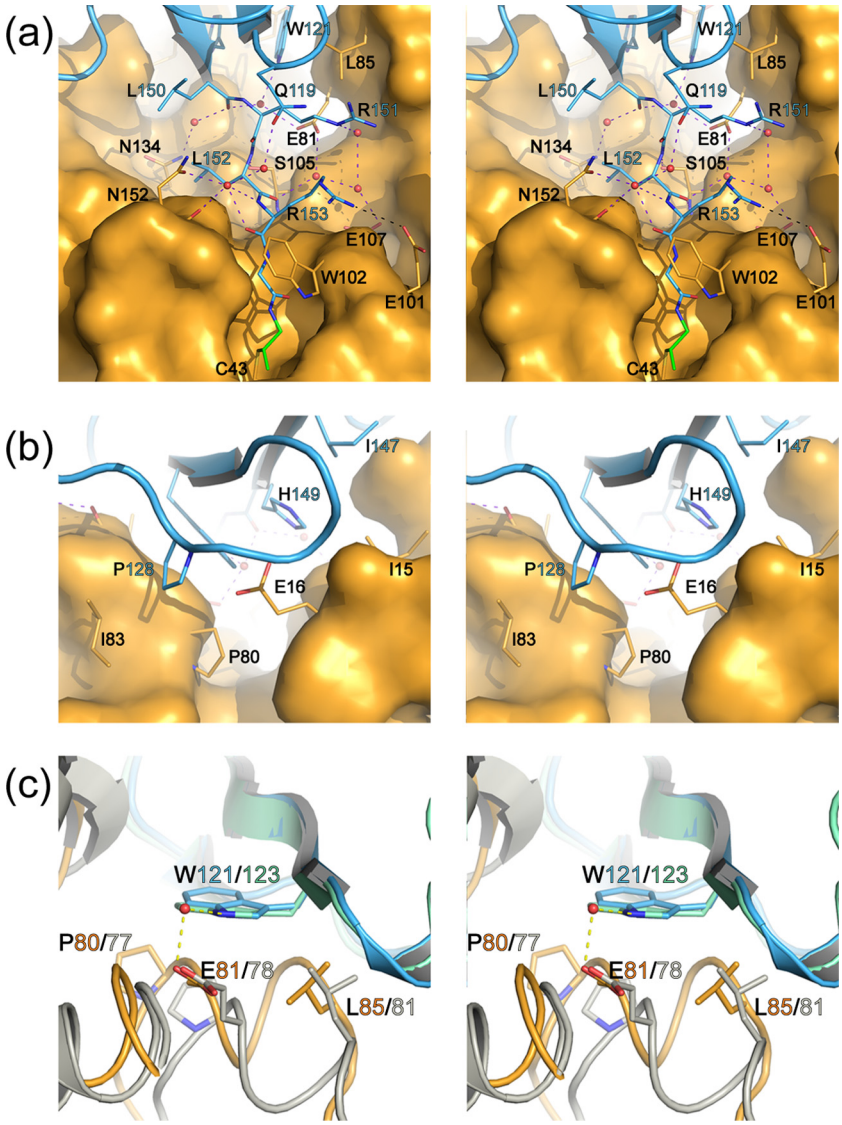

FIG 6 Interface of ERVV vOTU and CmISG15. (a) Wall-eye stereo view of the CmISG15 (blue cartoon) interactions leading to the active site of ERVV vOTU (orange surface). Hydrogen bond interactions are shown by purple dashes, salt bridges by black dashes. Distances of the electrostatic interactions shown range from 2.7 to 3.4 Å. (b) Wall-eye stereo view of peripheral hydrophobic interactions between CmISG15 and ERVV vOTU. (c) Wall-eye stereo view of the accommodation of Trp121 in the ERVV vOTU-CmISG15 and CCHFV vOTU-ChISG15 complexes (PDB code 3PHX). ERVV vOTU (orange) and CCHFV vOTU (gray) are shown as ribbons.

doubtful (Fig. 7a). In addition, CCHFV vOTU relies on F149 to fit into a hydrophobic pocket created by the CCHFV vOTU residue side chains of Val12 and Val18 as well as the methyl group on Thr10. At the mISG15 position equivalent to Phe149, there too is a hydrophobic residue. However, instead of the bulkier and longer phenylalanine, mISG15 has Ile147, which appears to be less likely to create the hydrophobic interaction seen in the CCHFV vOTU-hISG15 structure. Apart from these, the change from an Asn151 in hISG15 to its counterpart His149 in mISG15 would appear to create a steric clash with CCHFV vOTU residue Val18 if CCHFV vOTU were to engage mISG15 in a manner similar to that of hISG15. As the divergence at these three positions between mISG15 and hISG15 includes the interplay of differences in hydrogen bond interactions, hydrophobicity, and steric volume within a close proximity to each other, the impact of these particular sites on weaker mISG15 affinity for CCHFV vOTU likely could be synergistic.

Biodiversity of ISG15s and its impact on nairovirus vOTU deISGylase activities. Curiously, the divergence at positions equivalent to hISG15 89, 149, and 151 is not limited to only hISG15 and mISG15. When viewing the biodiversity of human, mouse, sheep, northern tree shrew, camel, and brown bat ISG15s using Consurf, the diversity at these positions among the six ISG15s tested as low to medium (Fig. 6b). Looking from a different perspective, no two of the six share homology at all three positions. Expanding the search to predicted ISG15s, an even greater diversity can be observed.

Excitingly, the level of homology among the ISG15s appears to correlate with their observed biochemical activity. For instance, ISG15s from humans and sheep are the closest in terms of simi-

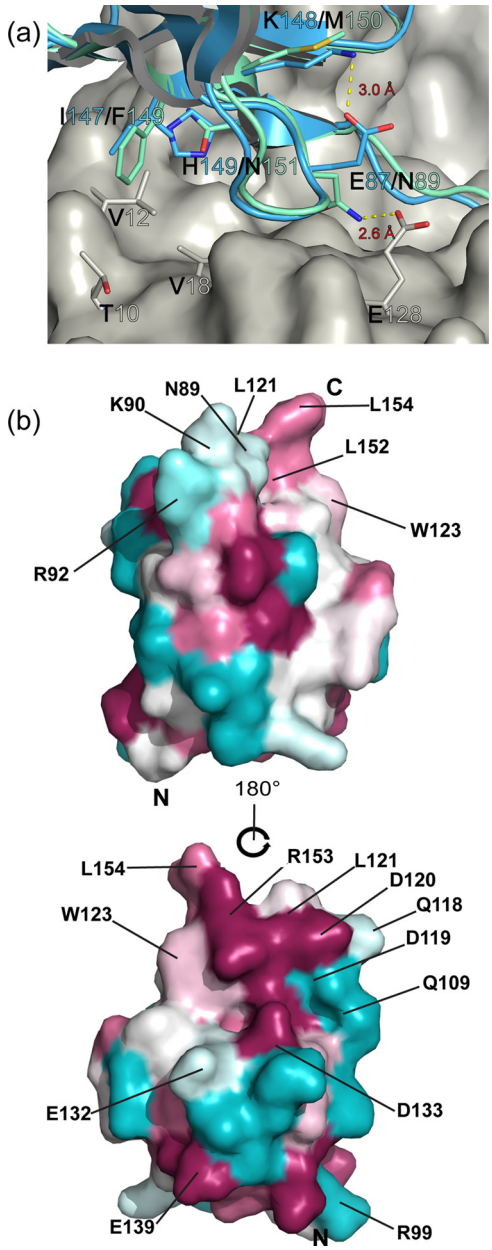

FIG 7 Potential impact of primary sequence differences on binding. (a) Internal changes altering interaction of substrate with vOTU. CmISG15 is shown in blue, ChISG15 in green. CCHFV vOTU from 3PHX is shown in gray. (b) Consurf surface rendering of conserved residues in the C-terminal lobe of human, sheep, northern tree shrew, mouse, camel, and bat ISG15s with human ISG15 as the reference structure. Sequences were derived from the same sources as those in Fig. 1b. Variable regions are shown in teal, conserved residues in burgundy.

larity at these three positions, with NFN and DFN, respectively (Fig. 1). The vOTUs from ERVV, CCHFV, and NSDV, which show strong affinity for pro-hISG15, also appear to robustly cleave pro-shISG15 (Fig. 2). In contrast, when the homology among these positions wanes, such as in the northern tree shrew ISG15, with a DYH motif in these positions, similarity in activities between ERVV, CCHFV, and NSDV vOTUs toward this ISG15 vary. Examining the sequence homology of the three positions and corresponding biochemical activity of the jackknife fish ISG15 adds further support for this concept. The fISG15 possesses an LHV motif at hISG15-equivalent positions 89, 149, and 151 as well as no measurable cleavage of the pro-fISG15 by the three nairovirus vOTUs tested. Although the interfaces of ERVV vOTU-CmISG15 and CCHFV vOTU highlight a number of residues responsible for their interfaces, the biochemical results appear to suggest that for nairovirus vOTUs, divergence at hISG15 positions 89, 149, and 151 plays a significant role in determining compatibility. As a result, observed differences at these positions could provide a blueprint for relative nairovirus deISGylase activity if a nairovirus vOTU has shown deISGylase activity for one species' ISG15.

Nairovirus vOTUs have been shown to interact only with the C-terminal domain of ISG15, a domain that tends to be more conserved then their N-terminal lobe counterpart (Fig. 1). In contrast, a coronavirus papain-like proteases (PLpro) was recently shown to interact with the N-terminal lobe (45). This suggests that these proteases, along with other host proteins that engage the N-terminal ISG15 lobe in addition to the C-terminal lobe, could exhibit even greater variances in their abilities to cleave ISG15 conjugates originating from different species.

The study of the large divergence in activities of proteases for certain species' ISG15s has been impeded, as tools to examine the impact of ISG15 biodiversity on enzymes have been unavailable until now. Previously, deISGylase activity was largely tied to the ability of a viral protease to cleave the human variant of ISG15 attached to 7-amino-4-methylcoumarin. This has led to the classification of many viral proteases as solely deubiquitinases. With nairoviruses exhibiting wide differences in the ability to cleave certain species' ISG15s, we propose that some proteases that exhibit only weak, or no, affinity for hISG15 may possess deISGylase activity for other species' ISG15s. This would stress that testing a wide range of ISG15s from various species will be necessary to clarify if their deISGylase is specific to particular species.

Currently, there is a dearth of information surrounding the full extent of the biodiversity of ISG15 in animals and the propensity of nairoviruses to replicate in or cause disease among vertebrates. Most nairoviruses can establish a persistent infection in ticks (46, 47). In contrast to the lifelong infection of tick host reservoirs, certain vertebrate hosts parasitized by ticks carrying CCHFV usually develop only transient viremia (46). Since no ISG15 homologues appear to exist in ticks, likely deISGylase activity is conserved to evade the immune response of vertebrate hosts and could be critical for virus transmission from ticks to certain species and its maintenance in nature. Linking the efficacy of vOTUs to engage a certain species ISG15 for a nairovirus to replicate or cause disease in vertebrates is not fully straightforward, as many factors are required for a virus to successfully infect a host. For example, ERVV was isolated from a white-tooth shrew and its vOTU is not able to cleave ISG15 originating from the northern tree shrew. This could be the result of differences in ISG15 between the white-tooth shrew and its northern tree shrew counterpart, but this issue cannot be directly resolved, as there is no sequence available for the white-tooth shrew. Erve virus belongs to the recently identified Thiafora genogroup, which comprises only two nairoviruses (Thiafora virus and ERVV) (3). Interestingly, both viruses were isolated from shrews and no tick or insect vector could be identified (23, 26). Therefore, shrew species could act as a reservoir for the Thiafora genogroup and deISGylase activity could be silent in the reservoir host. However, trends can be ob-

served for tick-borne nairovirus vOTUs that originate from viruses known to cause viremia or disease in a certain species and vigorously cleave the said species of ISG15. For example, ERVV vOTU robustly cleaves ISG15 from mice and humans, in which ERVV causes subdermal hemorrhaging and is implicated in thunderclap headaches, respectively (22–24). NSDV appears to have the most robust activity for ISG15 originating from sheep, but it can also cleave ISG15 from humans, in whom it also causes disease (18). This along with CCHFV vOTU's weaker affinity for mISG15 over hISG15 may suggest that there is a certain threshold of deISGylase activity needed to impact disease outcome from a vOTU perspective. At a minimum, this trend would propose that there is some evolutionary pressure for tick-borne nairoviruses to possess vOTUs that are optimized to ISG15 of susceptible vertebrate species.

ACKNOWLEDGMENTS

X-ray data were collected at Southeast Regional Collaborative Access Team (SER-CAT) 22-BM beamline at the Advanced Photon Source, Argonne National Laboratory. Supporting institutions may be found at http://www.ser-cat.org/members.html. Use of the Advanced Photon Source was supported by the U.S. Department of Energy, Office of Science, Office of Basic Energy Sciences, under contract no. W-31-109-Eng-38.

We thank Brittany Jenkins for carrying out the pro-ISG15 assay.

FUNDING INFORMATION

This work, including the efforts of Eric Bergeron and Scott D. Pegan, was funded by HHS | National Institutes of Health (NIH) (R01AI109008). This work, including the efforts of Scott D. Pegan, was funded by U.S. Department of Agriculture (USDA) (58-5030-5-034).

REFERENCES

1. **Cleaveland S, Laurenson MK, Taylor LH.** 2001. Diseases of humans and their domestic mammals: pathogen characteristics, host range and the risk of emergence. Philos Trans R Soc Lond B Biol Sci **356:**991–999. http://dx.doi.org/10.1098/rstb.2001.0889.
2. **Weaver SC, Reisen WK.** 2010. Present and future arboviral threats. Antiviral Res **85:**328–345. http://dx.doi.org/10.1016/j.antiviral.2009.10.008.
3. **Walker PJ, Widen SG, Wood TG, Guzman H, Tesh RB, Vasilakis N.** 2016. A global genomic characterization of nairoviruses identifies nine discrete genogroups with distinctive structural characteristics and host-vector associations. Am J Trop Med Hyg **94:**1107–1122. http://dx.doi.org/10.4269/ajtmh.15-0917.
4. **Weber F, Mirazimi A.** 2008. Interferon and cytokine responses to Crimean Congo hemorrhagic fever virus; an emerging and neglected viral zonoosis. Cytokine Growth Factor Rev **19:**395–404. http://dx.doi.org/10.1016/j.cytogfr.2008.11.001.
5. **Zhao C, Denison C, Huibregtse JM, Gygi S, Krug RM.** 2005. Human ISG15 conjugation targets both IFN-induced and constitutively expressed proteins functioning in diverse cellular pathways. Proc Natl Acad Sci U S A **102:**10200–10205. http://dx.doi.org/10.1073/pnas.0504754102.
6. **Frias-Staheli N, Giannakopoulos NV, Kikkert M, Taylor SL, Bridgen A, Paragas JJ, Richt JA, Rowland RR, Schmaljohn CS, Lenschow DJ, Snijder EJ, García-Sastre A, Virgin HW.** 2007. Ovarian tumor (OTU)-domain containing viral proteases evade ubiquitin- and ISG15-dependent innate immune responses. Cell Host Microbe **2:**404–416. http://dx.doi.org/10.1016/j.chom.2007.09.014.
7. **Xing Y, Chen J, Tu J, Zhang B, Chen X, Shi H, Baker SC, Feng L, Chen Z.** 2013. The papain-like protease of porcine epidemic diarrhea virus negatively regulates type I interferon pathway by acting as a viral deubiquitinase. J Gen Virol **94:**1554–1567. http://dx.doi.org/10.1099/vir.0.051169-0.
8. **Zheng D, Chen G, Guo B, Cheng G, Tang H.** 2008. PLP2, a potent deubiquitinase from murine hepatitis virus, strongly inhibits cellular type I interferon production. Cell Res **18:**1105–1113.
9. **Durfee LA, Lyon N, Seo K, Huibregtse JM.** 2010. The ISG15 conjugation system broadly targets newly synthesized proteins: implications for the antiviral function of ISG15. Mol Cell **38:**722–732. http://dx.doi.org/10.1016/j.molcel.2010.05.002.
10. **Ketscher L, Hannss R, Morales DJ, Basters A, Guerra S, Goldmann T, Hausmann A, Prinz M, Naumann R, Pekosz A, Utermohlen O, Lenschow DJ, Knobeloch KP.** 2015. Selective inactivation of USP18 isopeptidase activity in vivo enhances ISG15 conjugation and viral resistance. Proc Natl Acad Sci U S A **112:**1577–1582. http://dx.doi.org/10.1073/pnas.1412881112.
11. **Speer SD, Li Z, Buta S, Payelle-Brogard B, Qian L, Vigant F, Rubino E, Gardner TJ, Wedeking T, Hermann M, Duehr J, Sanal O, Tezcan I, Mansouri N, Tabarsi P, Mansouri D, Francois-Newton V, Daussy CF, Rodriguez MR, Lenschow DJ, Freiberg AN, Tortorella D, Piehler J, Lee B, Garcia-Sastre A, Pellegrini S, Bogunovic D.** 2016. ISG15 deficiency and increased viral resistance in humans but not mice. Nat Commun **7:**11496. http://dx.doi.org/10.1038/ncomms11496.
12. **Lai C, Struckhoff JJ, Schneider J, Martínez-Sobrido L, Wolff T, García-Sastre A, Zhang D-E, Lenschow DJ.** 2009. Mice lacking the ISG15 E1 enzyme UbE1L demonstrate increased susceptibility to both mouse-adapted and non-mouse-adapted influenza B virus infection. J Virol **83:**1147–1151. http://dx.doi.org/10.1128/JVI.00105-08.
13. **Sridharan H, Zhao C, Krug RM.** 2010. Species specificity of the NS1 protein of influenza B virus: it binds only human and non-human primate ubiquitin-like ISG15 proteins. J Biol Chem **285:**7852–7856. http://dx.doi.org/10.1074/jbc.C109.095703.
14. **Versteeg GA, García-Sastre A.** 2010. Viral tricks to grid-lock the type I interferon system. Curr Opin Microbiol **13:**508–516. http://dx.doi.org/10.1016/j.mib.2010.05.009.
15. **Barretto N, Jukneliene D, Ratia K, Chen Z, Mesecar AD, Baker SC.** 2005. The papain-like protease of severe acute respiratory syndrome coronavirus has deubiquitinating activity. J Virol **79:**15189–15198. http://dx.doi.org/10.1128/JVI.79.24.15189-15198.2005.
16. **Capodagli GC, Deaton MK, Baker EA, Lumpkin RJ, Pegan SD.** 2013. Diversity of ubiquitin and ISG15 specificity among nairoviruses' viral ovarian tumor domain proteases. J Virol **87:**3815–3827. http://dx.doi.org/10.1128/JVI.03252-12.
17. **Bergeron É, Albariño CG, Khristova ML, Nichol ST.** 2010. Crimean-Congo hemorrhagic fever virus-encoded ovarian tumor protease activity is dispensable for virus RNA polymerase function. J Virol **84:**216–226. http://dx.doi.org/10.1128/JVI.01859-09.
18. **Holzer B, Bakshi S, Bridgen A, Baron MD.** 2011. Inhibition of interferon induction and action by the nairovirus Nairobi sheep disease virus/Ganjam virus. PLoS One **6:**e28594. http://dx.doi.org/10.1371/journal.pone.0028594.
19. **Davies FG.** 1978. A survey of Nairobi sheep disease antibody in sheep and goats, wild ruminants and rodents within Kenya. J Hyg (Lond) **81:**251–258. http://dx.doi.org/10.1017/S0022172400025080.
20. **Schwarz TF, Nsanze H, Ameen AM.** 1997. Clinical features of Crimean-Congo haemorrhagic fever in the United Arab Emirates. Infection **25:**364–367. http://dx.doi.org/10.1007/BF01740819.
21. **Swanepoel R, Gill DE, Shepherd AJ, Leman PA, Mynhardt JH, Harvey S.** 1989. The clinical pathology of Crimean-Congo hemorrhagic fever. Rev Infect Dis **11**(Suppl 4)**:**S794–S800.
22. **Treib J, Dobler G, Haass A, von Blohn W, Strittmatter M, Pindur G, Froesner G, Schimrigk K.** 1998. Thunderclap headache caused by Erve virus? Neurology **50:**509–511. http://dx.doi.org/10.1212/WNL.50.2.509.
23. **Chastel C, Main AJ, Richard P, Le Lay G, Legrand-Quillien MC, Beaucoumu JC.** 1989. Erve virus, a probable member of Bunyaviridae family isloated from shrews (Crocidura russula) in France. Acta Virol **33:**270–280.
24. **Woessner R, Grauer MT, Langenbach J, Dobler G, Kroeger J, Mielke HG, Mueller P, Haass A, Treib J.** 2000. The Erve virus: possible mode of transmission and reservoir. Infection **28:**164–166. http://dx.doi.org/10.1007/s150100050072.
25. **Nalca AWC, Ergonul O, Whitehouse CA (ed).** 2007. Crimean-Congo hemorrhagic fever. Springer, Dordrecht, Netherlands.
26. **Dilcher M, Koch A, Hasib L, Dobler G, Hufert FT, Weidmann M.** 2012. Genetic characterization of Erve virus, a European nairovirus distantly related to Crimean-Congo hemorrhagic fever virus. Virus Genes **45:**426–432. http://dx.doi.org/10.1007/s11262-012-0796-8.
27. **Deaton MK, Spear A, Faaberg KS, Pegan SD.** 2014. The vOTU domain of highly-pathogenic porcine reproductive and respiratory syndrome virus displays a differential substrate preference. Virology **454-455:**247–253.
28. **Ekkebus R, van Kasteren SI, Kulathu Y, Scholten A, Berlin I, Geurink**

PP, de Jong A, Goerdayal S, Neefjes J, Heck AJR, Komander D, Ovaa H. 2013. On terminal alkynes that can react with active-site cysteine nucleophiles in proteases. J Am Chem Soc **135:**2867–2870. http://dx.doi.org/10.1021/ja309802n.

29. **Messick TE, Russell NS, Iwata AJ, Sarachan KL, Shiekhattar R, Shanks JR, Reyes-Turcu FE, Wilkinson KD, Marmorstein R.** 2008. Structural basis for ubiquitin recognition by the Otu1 ovarian tumor domain protein. J Biol Chem **283:**11038–11049. http://dx.doi.org/10.1074/jbc.M704398200.
30. **Wilkinson KD, Gan-Erdene T, Kolli N.** 2005. Derivitization of the C-terminus of ubiquitin and ubiquitin-like proteins using intein chemistry: methods and uses. Methods Enzymol **399:**37–51. http://dx.doi.org/10.1016/S0076-6879(05)99003-4.
31. **Otwinowski Z, Minor W.** 1997. Processing of X-ray diffraction data collected in oscillation mode. Methods Enzymol **276:**307–326.
32. **McCoy AJ, Grosse-Kunstleve RW, Adams PD, Winn MD, Storoni LC, Read RJ.** 2007. Phaser crystallographic software. J Appl Crystallogr **40:**658–674. http://dx.doi.org/10.1107/S0021889807021206.
33. **Emsley P, Cowtan K.** 2004. Coot: model-building tools for molecular graphics. Acta Crystallogr D Biol Crystallogr **60:**2126–2132. http://dx.doi.org/10.1107/S0907444904019158.
34. **Winn MD, Ballard CC, Cowtan KD, Dodson EJ, Emsley P, Evans PR, Keegan RM, Krissinel EB, Leslie AGW, McCoy A, McNicholas SJ, Murshudov GN, Pannu NS, Potterton EA, Powell HR, Read RJ, Vagin A, Wilson KS.** 2011. Overview of the CCP4 suite and current developments. Acta Crystallogr D Biol Crystallogr **67:**235–242. http://dx.doi.org/10.1107/S0907444910045749.
35. **Geurink PP, El Oualid F, Jonker A, Hameed DS, Ovaa H.** 2012. A general chemical ligation approach towards isopeptide-linked ubiquitin and ubiquitin-like assay reagents. Chembiochem **13:**293–297. http://dx.doi.org/10.1002/cbic.201100706.
36. **Müller MA, Devignot S, Lattwein E, Corman VM, Maganga GD, Gloza-Rausch F, Binger T, Vallo P, Emmerich P, Cottontail VM, Tschapka M, Oppong S, Drexler JF, Weber F, Leroy EM, Drosten C.** 2016. Evidence for widespread infection of African bats with Crimean-Congo hemorrhagic fever-like viruses. Sci Rep **6:**26637. http://dx.doi.org/10.1038/srep26637.
37. **Spengler JR, Bergeron E, Rollin PE.** 2016. Seroepidemiological studies of Crimean-Congo hemorrhagic fever virus in domestic and wild animals. PLoS Negl Trop Dis **10:**e0004210. http://dx.doi.org/10.1371/journal.pntd.0004210.
38. **Walker PJ, Widen SG, Firth C, Blasdell KR, Wood TG, Travassos da Rosa AP, Guzman H, Tesh RB, Vasilakis N.** 2015. Genomic characterization of Yogue, Kasokero, Issyk-Kul, Keterah, Gossas, and Thiafora viruses: nairoviruses naturally infecting bats, shrews, and ticks. Am J Trop Med Hyg **93:**1041–1051. http://dx.doi.org/10.4269/ajtmh.15-0344.
39. **Eisenmesser EZ, Capodagli GC, Armstrong GS, Holliday MJ, Isern NG, Zhang F, Pegan SD.** 2015. Inherent dynamics within the Crimean-Congo hemorrhagic fever virus protease are localized to the same region as substrate interactions. Protein Sci **24:**651–660. http://dx.doi.org/10.1002/pro.2637.
40. **Dolinsky TJ, Nielsen JE, McCammon JA, Baker NA.** 2004. PDB2PQR: an automated pipeline for the setup of Poisson-Boltzmann electrostatics calculations. Nucleic Acids Res **32:**W665–W667. http://dx.doi.org/10.1093/nar/gkh381.
41. **Narasimhan J, Wang M, Fu Z, Klein JM, Haas AL, Kim JJ.** 2005. Crystal structure of the interferon-induced ubiquitin-like protein ISG15. J Biol Chem **280:**27356–27365. http://dx.doi.org/10.1074/jbc.M502814200.
42. **Akutsu M, Ye Y, Virdee S, Chin JW, Komander D.** 2011. Molecular basis for ubiquitin and ISG15 cross-reactivity in viral ovarian tumor domains. Proc Natl Acad Sci U S A **108:**2228–2233. http://dx.doi.org/10.1073/pnas.1015287108.
43. **James TW, Frias-Staheli N, Bacik JP, Levingston Macleod JM, Khajehpour M, Garcia-Sastre A, Mark BL.** 2011. Structural basis for the removal of ubiquitin and interferon-stimulated gene 15 by a viral ovarian tumor domain-containing protease. Proc Natl Acad Sci U S A **108:**2222–2227. http://dx.doi.org/10.1073/pnas.1013388108.
44. **Ishii A, Ueno K, Orba Y, Sasaki M, Moonga L, Hang'ombe BM, Mweene AS, Umemura T, Ito K, Hall WW, Sawa H.** 2014. A nairovirus isolated from African bats causes haemorrhagic gastroenteritis and severe hepatic disease in mice. Nat Commun **5:**5651. http://dx.doi.org/10.1038/ncomms6651.
45. **Ratia K, Kilianski A, Baez-Santos YM, Baker SC, Mesecar A.** 2014. Structural basis for the ubiquitin-linkage specificity and deISGylating activity of SARS-CoV papain-like protease. PLoS Pathog **10:**e1004113. http://dx.doi.org/10.1371/journal.ppat.1004113.
46. **Bente DA, Forrester NL, Watts DM, McAuley AJ, Whitehouse CA, Bray M.** 2013. Crimean-Congo hemorrhagic fever: history, epidemiology, pathogenesis, clinical syndrome and genetic diversity. Antiviral Res **100:**159–189. http://dx.doi.org/10.1016/j.antiviral.2013.07.006.
47. **Booth TF, Steele GM, Marriott AC, Nuttall PA.** 1991. Dissemination, replication, and trans-stadial persistence of Dugbe virus (Nairovirus, Bunyaviridae) in the tick vector Amblyomma variegatum. Am J Trop Med Hyg **45:**146–157.